Cai et al. Nanoscale Research Letters (2015) 10:126
DOI 10.1186/s11671-015-0825-3

Nanoscale Research Letters
a SpringerOpen Journal

NANO EXPRESS Open Access

First-principles calculations of perpendicular magnetic anisotropy in $Fe_{1-x}Co_x$/MgO(001) thin films

Guanzhi Cai, Zhiming Wu, Fei Guo, Yaping Wu, Heng Li, Qianwen Liu, Mingming Fu, Ting Chen* and Junyong Kang*

Abstract

The perpendicular magnetic anisotropy (PMA) of $Fe_{1-x}Co_x$ thin films on MgO(001) was investigated via first-principles density-functional calculations. Four different configurations were considered based on their ground states: Fe/MgO, $Fe_{12}Co_4$/MgO, $Fe_{10}Co_6$/MgO, and Fe_8Co_8/MgO. As the Co composition increases, the amplitude of PMA increases first from Fe/MgO to $Fe_{12}Co_4$/MgO, and then decreases in $Fe_{10}Co_6$/MgO; finally, the magnetic anisotropy becomes horizontal in Fe_8Co_8/MgO. Analysis based on the second-order perturbation of the spin-orbit interaction was carried out to illustrate the contributions from Fe and Co atoms to PMA, and the differential charge density was calculated to give an intuitive comparison of 3*d* orbital occupancy. The enhanced PMA in $Fe_{12}Co_4$/MgO is ascribed to the optimized combination of occupied and unoccupied 3*d* states around the Fermi energy from both interface Fe and Co atoms, while the weaker PMA in $Fe_{10}Co_6$/MgO is mainly attributed to the modulation of the interface Co-d_{xy} orbital around the Fermi energy. By adjusting the Co composition in $Fe_{1-x}Co_x$, the density of states of transitional metal atoms will be modulated to optimize PMA for future high-density memory application.

Keywords: First-principles calculations; FeCo/MgO; Perpendicular magnetic anisotropy

Background

Materials with large magnetic moments and strong perpendicular magnetic anisotropy (PMA) are of great interest due to their potential applications in next-generation high-density non-volatile memories and high thermal stability logic chips [1-6]. Numbers of materials with strong PMA have been explored during the past decades, such as $L1_0$-ordered (Co,Fe)-Pt alloys [7-9], Co/(Pd,Pt) multilayers [10-12], and $D0_{22}$-ordered $Mn_{3-\delta}Ga$ [13,14]. However, none of them satisfy the high thermal stability, low switching current, and high tunnel magnetoresistance (TMR) ratio at the same time. Recently, FeCo alloys with high saturation magnetization, high Curie temperature, good permeability, and large magnetocrystalline anisotropy energy have been paid great attention [15]. The large values of uniaxial magnetocrystalline anisotropy energy (K_u) and saturation magnetization (M_s) were first predicted by Burkert et al. via first-principles calculations [16] and then verified by experiments [17,18]. Particularly, S. Ikeda et al. obtained Ta/FeCoB/MgO/FeCoB/Ta perpendicular magnetic tunnel junctions with high TMR ratio (over 120%), high thermal stability at a dimension of 40 nm diameter, and a low switching current of 49 μA [19], revealing a promising building block for future high-density memories. After that, lots of experiments based on $Fe_{1-x}Co_x$/MgO magnetic tunnel junctions have been performed to explore the influence of growth regulation, electric field, Fe-Co proportion, and so on [20-23]. Though it has been proved by experiments that Fe-rich $Fe_{1-x}Co_xB$/MgO structures have larger PMA than their Co-rich counterparts, there is short of theoretical guidance for optimizing Fe-Co proportion, and the inherent origin of PMA in $Fe_{1-x}Co_xB$/MgO is still unclear.

* Correspondence: ting.chen@xmu.edu.cn; jykang@xmu.edu.cn
Department of Physics, Fujian Key Laboratory of Semiconductor Materials and Applications, Xiamen University, 422 Siming South Road, Xiamen 361005, People's Republic of China

In this work, we investigated the amplitude of PMA depending on the cobalt composition and explored the origin of PMA in $Fe_{1-x}Co_x$/MgO magnetic tunnel junctions via first-principles calculations. Second-order perturbation theory was adopted to illustrate the contributions from Fe and Co atoms to PMA. The differential charge density at the sites where Co atoms take the place of Fe atoms was calculated to give an intuitive comparison of 3*d* orbital occupancy. By adjusting the cobalt composition, the density of states (DOS) will be modulated, and strong PMA will be obtained with an optimized combination of occupied and unoccupied 3*d* states around the Fermi energy (E_F).

Methods

We performed first-principles density-functional calculations using the Vienna *ab initio* simulation package (VASP) with the consideration of the spin-orbit interactions. For the electronic exchange-correlation and electron-ion interaction, we adopted the spin-polarized generalized gradient approximation (GGA) [24] and the projector-augmented wave (PAW) potential [25], respectively. A 9 × 9 × 1 *k*-point mesh was used with the energy cutoff equal to 500 eV. Four 2 × 2 supercells with different Co concentrations were considered in this work: Fe/MgO(001), $Fe_{12}Co_4$/MgO(001), $Fe_{10}Co_6$/MgO (001), and Fe_8Co_8/MgO(001) (Figure 1). The configurations of FeCo alloys were given as their ground states according to previous work, i.e., $L1_0$-$Fe_{12}Co_4$, $Fe_{10}Co_6$, and B2-Fe_8Co_8 (CsCl type) [26]. Along the *z*-axis, there were three MgO monolayers, four $Fe_{1-x}Co_x$ monolayers and 15 Å vacuum. Each supercell includes 40 atoms. The bottom MgO monolayer was fixed as bulk, and the in-plane lattice constant of the supercell was fixed at $\sqrt{2}$a (cubic MgO: a = 4.212 Å) since a thin ferromagnetic layer was used. All the other layers were fully relaxed until the largest force between the atoms worked out to be less than 1 meV/Å. The magnetic anisotropy energy (MAE) was calculated by taking the difference between the total energy of the magnetization oriented along the in-plane [100] and out-of-plane [001] directions based on the force theorem.

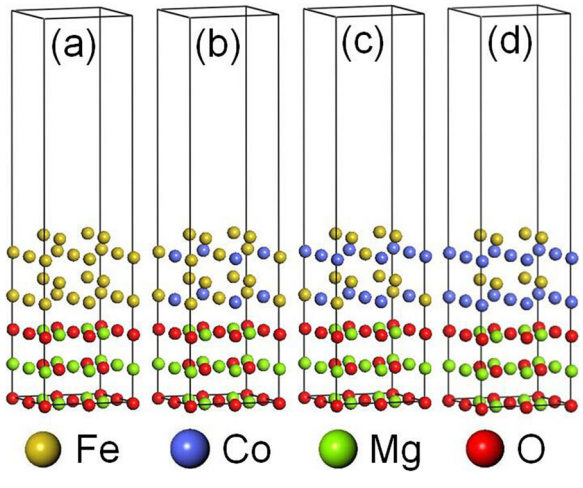

Figure 1 Schematics of the calculated structures. (a) Fe/MgO, **(b)** $Fe_{12}Co_4$/MgO, **(c)** $Fe_{10}Co_6$/MgO, and **(d)** Fe_8Co_8/MgO. Fe, Co, Mg, and O atoms are represented by yellow, blue, green, and red balls, respectively.

Results and discussion

The calculated MAE in $Fe_{1-x}Co_x$/MgO (x = 0, 0.25, 0.375, 0.5) configurations are listed in Table 1. Fe/MgO, $Fe_{12}Co_4$/MgO, and $Fe_{10}Co_6$/MgO have a positive MAE of 4.2, 7.1, and 3.3 meV, respectively, indicating the preference of out-of-plane magnetization. However, Fe_8Co_8/MgO has a negative MAE of −17.1 meV, showing an in-plane easy magnetization. In Fe_8Co_8/MgO, the interfacial Fe atoms are replaced by Co atoms, and the calculated magnetic moment of O atoms in Co-O bonds is 0.013 μ_B, only half of that in Fe-O bonds (0.025 μ_B), indicating the reduced transition metal-oxygen hybridization. As revealed by Yang et al., the hybridization between Fe and O atoms at interface greatly contributed to PMA in Fe/MgO [27]. Thus, the attenuated interface hybridization in Fe_8Co_8/MgO may be an origin of the in-plane easy magnetization. Furthermore, for FeCo monolayers epitaxially grown on MgO (001), the in-plane lattice is enlarged to match that of MgO(001) (a = 2.97 Å), while the out-of-plane lattice is shortened to 2.71 Å, leading to a c/a ratio of 0.91. It has been reported that the MAE reduces as the c/a ratio decreases and becomes negative when it is smaller than 1 for B2-FeCo alloy [28]. Hence, a negative MAE is anticipated in Fe_8Co_8/MgO. In a word, the replacement of interface Fe atoms with Co atoms and the small c/a ratio in Fe_8Co_8/MgO accounts for the in-plane magnetization.

Note that $Fe_{12}Co_4$/MgO has the largest PMA value, implying that a proper Fe-Co combination will enhance PMA. It has been reported that the PMA is dominated by the interfacial anisotropy in $Fe_{1-x}Co_x$/MgO systems [19]. Furthermore, the Fe-O hybridization makes the primary contribution to PMA in Fe/MgO systems. As

Table 1 MAE values and interfacial distances of Fe-O and Co-O bonds in $Fe_{1-x}Co_x$/MgO systems

	Distance (Fe-O Å)	Distance (Co-O Å)	MAE (meV)
Fe/MgO	2.136	\	4.2
$Fe_{12}CO_4$/MgO	2.073	2.164	7.1
$Fe_{10}CO_6$/MgO	2.079	2.127	3.3
Fe_8CO_8/MgO	\	2.103	−17.1

shown in Table 1, the Fe-O distances in Fe/MgO, $Fe_{12}Co_4$/MgO, and $Fe_{10}Co_6$/MgO are 2.136, 2.073, and 2.079 Å, respectively. The change of the Fe-O distance will cause the reconstruction of the electronic structure of Fe-d_{z^2} around the E_F. Figure 2 shows the DOS of Fe-d_{z^2} and O-p_z orbitals at Fe/MgO, $Fe_{12}Co_4$/MgO, and $Fe_{10}Co_6$/MgO interfaces. In the vicinity of E_F, there are enhanced hybridization peaks indicated by dashed lines in $Fe_{12}CO_4$/MgO and $Fe_{10}Co_6$/MgO, implying an increased occupancy of Fe-d_{z^2} states compared with Fe/MgO. Meanwhile, Fe-$d_{xz,yz}$ states hybridize with d_{z^2} states through spin-orbital interaction, leading to enhanced $d_{xz,yz}$ occupancy. According to the previous reports, $d_{xz,yz}$ orbital plays an important role in the out-of-plane components of PMA [27]. Therefore, the Fe atoms in $Fe_{12}Co_4$/MgO and $Fe_{10}Co_6$/MgO will somehow increase the positive contribution to PMA due to the enhanced Fe-O hybridization.

To further understand the contributions from Fe atoms to PMA in $Fe_{1-x}Co_x$/MgO systems, we consider the second-order perturbative contribution of spin-orbit coupling (SOC) to magnetocrystalline anisotropy energies $\left(E^{(2)}_{\mathrm{MCA}}\right)$ depending on the atomic site and the spin-transition process. $E^{(2)}_{\mathrm{MCA}}$ can be expressed by four terms

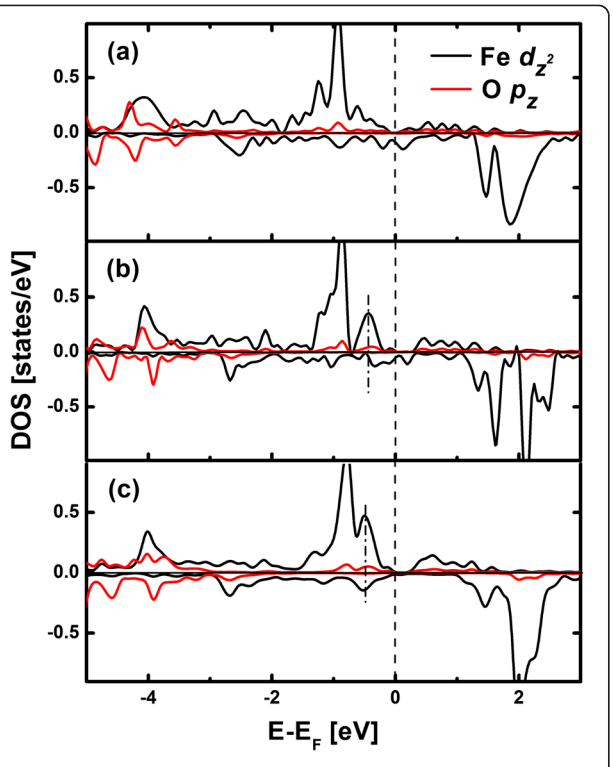

Figure 2 Majority-spin (positive) and minority-spin (negative) DOS of Fe-d_{z^2} and O-p_z. (a) Fe/MgO interface, **(b)** $Fe_{12}Co_4$/MgO interface, and **(c)** $Fe_{10}Co_6$/MgO interface as a function of energy relative to the *EF*.

(up-up, down-down, up-down, down-up) according to the Ref. [29]:

$$E^{(2)}_{\mathrm{MCA}} = \sum_i E^i_{\mathrm{MCA}} = \sum_i \Delta E^i_{\uparrow\Rightarrow\uparrow} + \Delta E^i_{\downarrow\Rightarrow\downarrow} - \Delta E^i_{\uparrow\Rightarrow\downarrow} - \Delta E^i_{\downarrow\Rightarrow\uparrow} \quad (1)$$

and

$$\Delta E^i_{\sigma\Rightarrow\sigma'} = -\xi_i \sum_{\mu\lambda\mu'\lambda'} [\lambda\uparrow|L_X|\lambda'\uparrow\mu'\uparrow|L_X|\mu\uparrow - \lambda\uparrow|L_Z|\lambda'\uparrow\mu'\uparrow|L_Z|\mu\uparrow] \times \sum_j \xi_j G^{\mu'\lambda'}_{\mu\lambda}\left(\sigma,\sigma';i,j\right) \quad (2)$$

where $\Delta E^i_{\uparrow\Rightarrow\uparrow}$ (up-up) in Equation 1 indicates a virtual excitation from occupied majority-spin states to unoccupied majority-spin states of an atom in the second-order perturbation. In Equation 2, ξ is the SOC constant, σ is the spin state, $\lambda(\mu)$ is the atomic orbital state, the superscript $'$ represents the unoccupied state, and $G^{\mu'\lambda'}_{\mu\lambda}\left(\sigma,\sigma';i,j\right)$ is an integral of the joint density of states given by

$$G^{\mu'\lambda'}_{\mu\lambda}\left(\sigma,\sigma';i,j\right) = \int_{-\infty}^{E_F} d\varepsilon \int_{-\infty}^{E_F} d\varepsilon' \frac{1}{\varepsilon'-\varepsilon} \times \sum_k \sum_n^{\mathrm{occ}} c^{kn*}_{i\mu\sigma} c^{kn}_{j\lambda\sigma} \delta\left(\varepsilon - \varepsilon^{(0)}_{kn\sigma}\right) \times \sum_{n'}^{\mathrm{unocc}} c^{kn'*}_{i\mu'\sigma'} c^{kn'}_{j\lambda'\sigma'} \delta\left(\varepsilon' - \varepsilon^{(0)}_{kn'\sigma'}\right) \quad (3)$$

where $c^{kn}_{i\mu\sigma}$ is the components of an orthogonal basis of atomic orbitals and $\varepsilon^{(0)}_{kn\sigma}$ is the energy of unperturbed state. It can be seen from Equations 2 and 3 that $\Delta E^i_{\sigma\Rightarrow\sigma'}$ depends not only on the coupling between the occupied states and unoccupied states but also strongly on the splitting between them through the energy denominator in Equation 3. As a result, $\Delta E^i_{\sigma\Rightarrow\sigma'}$ is mainly determined by the DOS in the vicinity of E_F. Figures 3a,b,c,d show the DOS of Fe d_{xy}, $d_{xz,yz}$, d_{z^2}, and $d_{x^2-y^2}$ at Fe/MgO, $Fe_{12}CO_4$/MgO, and $Fe_{10}Co_6$/MgO interfaces as a function of energy relative to E_F. The majority-spin states are almost fully occupied, and the minority-spin states are partially occupied for Fe d_{xy}, $d_{xz,yz}$, d_{z^2}, and $d_{x^2-y^2}$ orbitals. According to Equations 2 and 3, $\Delta E^{\mathrm{Fe}}_{\downarrow\Rightarrow\uparrow}$ (i.e., the coupling between occupied minority-spin states and unoccupied majority-spin states) and $\Delta E^{\mathrm{Fe}}_{\uparrow\Rightarrow\uparrow}$ (i.e., the coupling between occupied majority-spin states and unoccupied majority-spin states) can be neglected. The spin-flip term $\Delta E^{\mathrm{Fe}}_{\uparrow\Rightarrow\downarrow}$ and the spin-conservation term $\Delta E^{\mathrm{Fe}}_{\downarrow\Rightarrow\downarrow}$ make the main contributions to the MAE. To estimate $\Delta E^i_{\sigma\Rightarrow\sigma'}$, the angular momentum matrix elements are considered. Due to symmetry property of the atomic orbitals, only a few angular momentum matrix elements

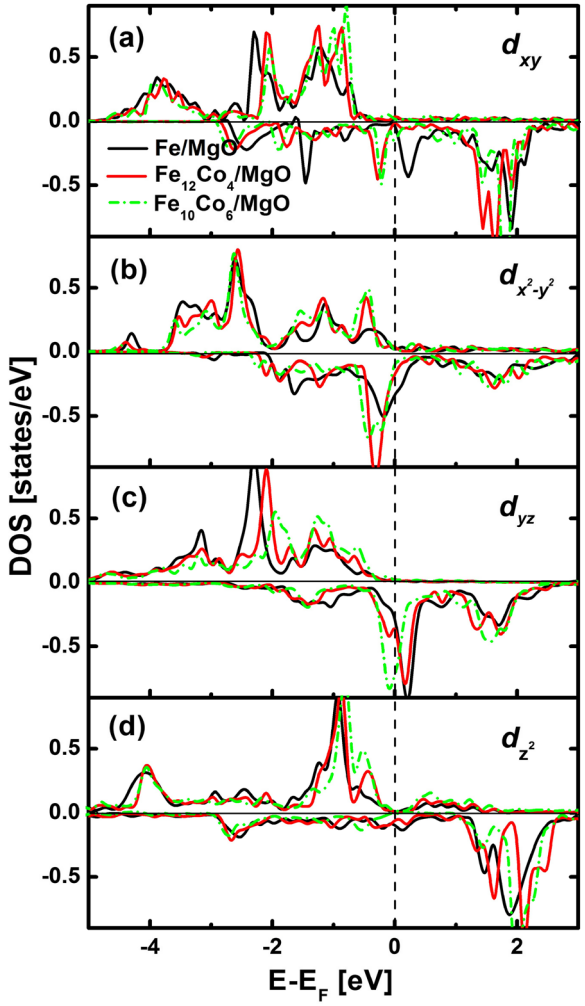

Figure 3 Majority-spin (positive) and minority-spin (negative) DOS projected to Fe-3*d* orbital components (a-d). Fe/MgO interface (black), $Fe_{12}Co_4$/MgO interface (red), and $Fe_{10}Co_6$/MgO interface (green).

between the d orbitals are nonzero: $\langle xz|L_z|yz\rangle$, $\langle x^2-y^2|L_z|xy\rangle$, $\langle z^2|L_x|yz\rangle$, $\langle xy|L_x|xz\rangle$, and $\langle x^2-y^2|L_x|yz\rangle$ (bra and ket can be exchanged). Among which, $\langle\mu|L_z|\mu'\rangle$ makes a positive contribution to PMA through spin-conservation term $\Delta E^i_{\downarrow\Rightarrow\downarrow}$ and a negative contribution through spin-flip term $\Delta E^i_{\uparrow\Rightarrow\downarrow}$, opposite does $\langle\mu|L_x|\mu'\rangle$. In Fe/MgO, the matrix element $\langle x^2-y^2|L_z|xy\rangle$ makes the main positive contribution to PMA due to the large occupied $d_{x^2-y^2}$ and unoccupied d_{xy} states of minority-spin around E_F. The primary negative contribution comes from $\langle x^2-y^2|L_x|yz\rangle$ and $\langle yz|L_x|x^2-y^2\rangle$ on account of large unoccupied d_{yz} states and relative large unoccupied $d_{x^2-y^2}$ states around E_F. To sum up, the PMA value contributed from all nonvanishing angular momentum matrix elements connecting d states $\pm|\mu'|L|\mu|^2 G^{\mu\mu'}_{\mu\mu}(\sigma,\downarrow;\mathrm{Fe},\mathrm{Fe})$ is positive. Different from Fe/MgO, the matrix elements $\langle x^2-y^2|L_z|xy\rangle$ in $Fe_{12}Co_4$/MgO and $Fe_{10}Co_6$/MgO are quite small because of the greatly reduced unoccupied minority-spin d_{xy} states. The other obvious changes are the increase of occupied minority-spin d_{yz} states in both $Fe_{12}Co_4$/MgO and $Fe_{10}Co_6$/MgO and the decrease of unoccupied minority-spin $d_{x^2-y^2}$ states, which will amplify the positive value of $\langle xz|L_z|yz\rangle$ and diminish the negative value of $\langle yz|L_x|x^2-y^2\rangle$. As a result, the contributions from Fe atoms in $Fe_{12}Co_4$/MgO and $Fe_{10}Co_6$/MgO to PMA are larger than those in Fe/MgO, which confirms the speculation based on Fe-O hybridization.

In the following, the contributions from Co atoms are taken into consideration. The DOS of Co-d_{xy}, $d_{xz,yz}$, d_{z^2}, and $d_{x^2-y^2}$ at $Fe_{12}Co_4$/MgO and $Fe_{10}Co_6$/MgO interfaces are shown in Figure 4a,b,c,d. Since Co atoms at $Fe_{10}Co_6$/MgO interface are not symmetrical, we present their DOS

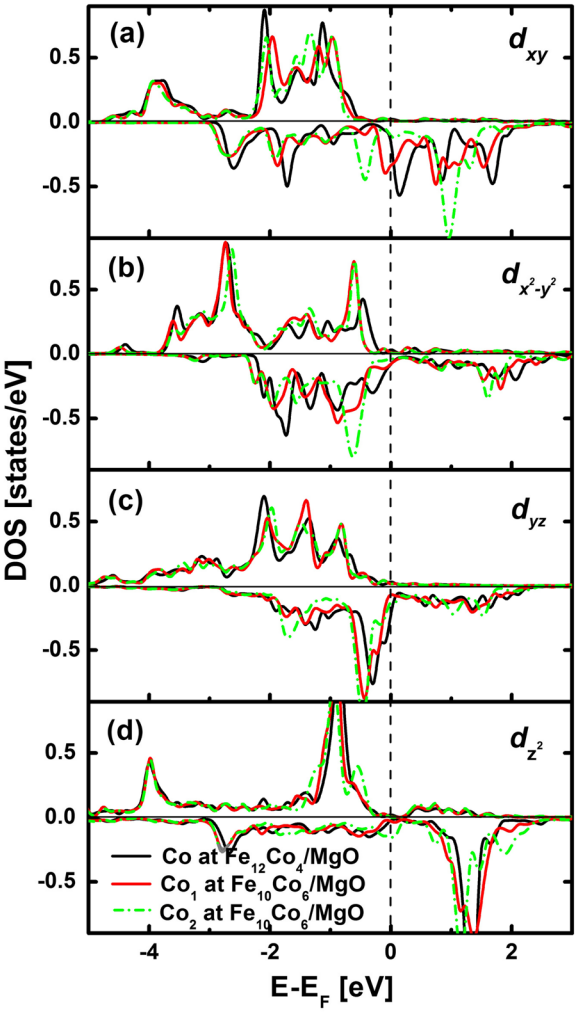

Figure 4 Majority-spin (positive) and minority-spin (negative) DOS projected to Co-3*d* orbital components (a-d). $Fe_{12}Co_4$/MgO interface (black) and $Fe_{10}Co_6$/MgO interface. Co_1 (red) represents the Co atom at the edge of the interface, and Co_2 (green) represents the Co atom in the center of the interface.

separately. Co_1 represents the Co atom at the edge of the interface, and Co_2 represents the Co atom in the center of the interface. Different from Fe-d_{yz} states, the unoccupied Co-d_{yz} states around E_F are relatively small in $Fe_{12}Co_4$/MgO; thus, the negative matrix element $\langle x^2-y^2|L_x|yz\rangle$ is much smaller than that of Fe/MgO. The other negative contribution arising from $\langle yz|L_x|xy\rangle$ is comparable to the negative matrix element $\langle yz|L_x|x^2-y^2\rangle$ in Fe/MgO. In addition, the positive contribution of L_z connecting occupied $d_{x^2-y^2}$ and unoccupied d_{xy} states in $Fe_{12}Co_4$/MgO is comparable to that in Fe/MgO. In general, Co atoms in $Fe_{12}Co_4$/MgO contribute much more to PMA than Fe atoms in Fe/MgO. In the light of these, the PMA value contributed from both Fe and Co atoms is much larger in $Fe_{12}Co_4$/MgO than in Fe/MgO. In $Fe_{10}Co_6$/MgO, the positive matrix element $\langle x^2-y^2|L_z|xy\rangle$ decreases due to the reduced unoccupied d_{xy} states for Co_1 atom. It deceases even more for Co_2 atom because of the very small unoccupied d_{xy} states. Consequently, the contribution from Co atoms in $Fe_{10}Co_6$/MgO is much smaller than Co atoms in $Fe_{12}Co_4$, resulting in a relative small value of PMA.

In order to give a more intuitive comparison of the contributions of Fe and Co atoms, we calculated the differential charge density. Figures 5a,b shows the differential charge density of $Fe_{12}Co_4$/MgO and Fe/MgO at the sites where Fe atoms are replaced by Co atoms at interface. Compared with Fe atoms in Fe/MgO, Co atoms in $Fe_{12}Co_4$/MgO have larger $d_{xz,yz}$ and d_{xy} occupancy but smaller $d_{x^2-y^2}$ and d_{z^2} occupancy. The occupancy of d_{z^2}, d_{xz}, and d_{yz} orbitals determine the atomic orbital magnetic moments of [001], while the occupancy of d_{xy} and $d_{x^2-y^2}$ orbitals contribute to [100] [30]. Due to the sharply reduced $d_{x^2-y^2}$ occupancy, Co atoms in $Fe_{12}Co_4$/MgO contribute more to PMA than Fe atoms in Fe/MgO, which is consistent with the estimation from the second-order perturbation of SOC. Figures 5c,d display the differential charge density of $Fe_{10}Co_6$/MgO and $Fe_{12}Co_4$/MgO at the center of the interface where Co atom replace Fe atom. The d_{z^2} occupancy increases, but the $d_{xz,yz}$ occupancy largely decreases. In addition, the d_{xy} states enhance dramatically. As a result, Co_2 atom in $Fe_{10}Co_6$/MgO contributes much less to PMA than Fe atom in $Fe_{12}Co_4$/MgO, which agrees well with the estimation from the second-order perturbation of SOC.

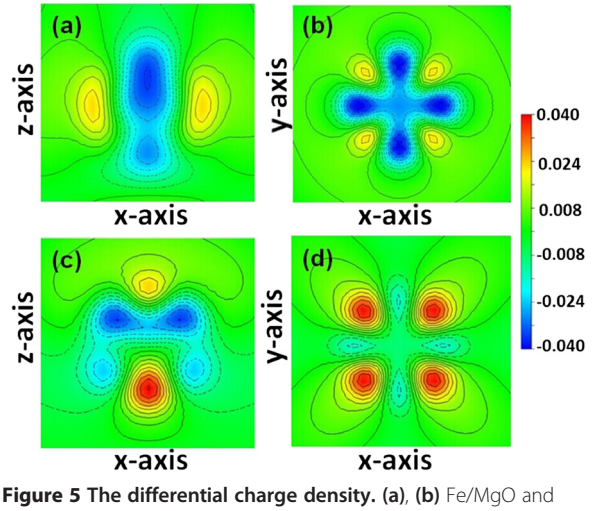

Figure 5 The differential charge density. (a), (b) Fe/MgO and $Fe_{12}Co_4$/MgO interfaces where Co take Fe site; **(c), (d)** $Fe_{12}Co_4$/MgO and $Fe_{10}Co_6$/MgO interfaces where extra Co take center Fe site.

Conclusions

In summary, we have presented first-principles studies of PMA in $Fe_{1-x}Co_x$/MgO as a function of the Co composition and strong PMA with an amplitude of 7.1 mV is discovered in $Fe_{12}Co_4$/MgO. The change of Co composition modulates the DOS of Fe and Co atoms around E_F and varies their contributions to PMA. The enhanced PMA in $Fe_{12}Co_4$/MgO is ascribed to the optimized combination of interface occupied and unoccupied 3*d* states around E_F, where both Fe and Co atoms make a large out-of-plane contribution and a small in-plane contribution. The weaker PMA in $Fe_{10}Co_6$/MgO is due to the sharply decreased unoccupied Co-d_{xy} states around E_F and dramatically increased Co-d_{xy} occupancy, where Co atoms especially the Co atom at the center of interface make a small out-of-plane contribution. The horizontal magnetic anisotropy in Fe_8Co_8/MgO is mainly resulted from the attenuation of interface hybridization and the small *c*/*a* ratio. Therefore, reasonable adjustment of Fe-Co combination in $Fe_{1-x}Co_x$/MgO magnetic tunnel junctions will enhance PMA and is worthy of further investigation. This work provides a basis method to investigate promising building blocks for future high-density memories.

Competing interests

The authors declare that they have no competing interests.

Authors' contributions

GZC carried out the experiments and drafted the manuscript. ZMW and FG helped to guide the calculations. YPW, HL, QWL, and MMF took part in the data analysis. Dr. TC and Prof. JYK participated in the conception of the project, improved the manuscript, and coordinated between all the participants. All authors read and approved the final manuscript.

Acknowledgments

This work was financially supported by the National Natural Science Foundation of China (Grant Nos. 61227009, 61106008, 61106118, and 11304257), the "973" Program (Grant Nos. 2011CB925600 and 2012CB619301), the Natural Science Foundation of Fujian Province of China (Grant No. 2014 J01026). This work was also supported partially by the Chinese Hungarian Intergovernmental S&T Cooperation Program (Project No: TÉT_12_CN-1-2012-0040, CH-6-26/2012).

Received: 30 November 2014 Accepted: 17 February 2015
Published online: 12 March 2015

References

1. Mangin S, Ravelosona D, Katine JA, Carey MJ, Terris BD. Current-induced magnetization reversal in nanopillars with perpendicular anisotropy. Nat Mater. 2006;5(3):210–5.
2. Thompson SM. The discovery, development and future of GMR: The Nobel Prize 2007. J Phys D Appl Phys. 2008;41(9):093001.
3. Kishi T, Yoda H, Kai T, Nagase T, Kitagawa E, Yoshikawa M, et al. Lower-current and fast switching of a perpendicular TMR for high speed and high density spin-transfer-torque MRAM. San Francisco, USA: Proceedings of IEEE International Electron Devices Meeting; 2008. p. 309–12.
4. Piramanayagam SN. Perpendicular recording media for hard disk drives. J Appl Phys. 2007;102(1):011301.
5. Ikeda S, Hayakawa J, Lee YM, Matsukura F, Ohno Y, Hanyu T, et al. Magnetic tunnel junctions for spintronic memories and beyond. Electron Devices, IEEE Trans. 2007;54(5):991–1002.
6. Weller D, Moser A, Folks L, Best ME, Lee W, Toney MF, et al. High K_u materials approach to 100 Gbits/in^2. Magnetics, IEEE Trans. 2000;36(1):10–5.
7. Rong C, Li D, Nandwana V, Poudyal N, Ding Y, Wang ZL, et al. Size-dependent chemical and magnetic ordering in $L1_0$-FePt nanoparticles. Adv Mater. 2006;18(22):2984–8.
8. Yoshikawa M, Kitagawa E, Nagase T, Daibou T, Nagamine M, Nishiyama K, et al. Tunnel magnetoresistance over 100% in MgO-based magnetic tunnel junction films with perpendicular magnetic $L1_0$-FePt electrodes. Magnetics, IEEE Trans. 2008;44(11):2573–6.
9. Kim G, Sakuraba Y, Oogane M, Miyazaki T. Tunneling magnetoresistance of magnetic tunnel junctions using perpendicular magnetization $L1_0$-CoPt electrodes. Appl Phys Lett. 2008;92(17):172502–2.
10. Park JH, Park C, Jeong T, Moneck MT, Nufer NT, Zhu JG. Co/Pt multilayer based magnetic tunnel junctions using perpendicular magnetic anisotropy. J Appl Phys. 2008;103.7:07A917.
11. Carvello B, Ducruet C, Rodmacq B, Auffret S, Gautier E, Gaudin G, et al. Sizable room-temperature magnetoresistance in cobalt based magnetic tunnel junctions with out-of-plane anisotropy. Appl Phys Lett. 2008;92(10):102508.
12. Koda T, Awano H, Hieda H, Naito K, Kikitsu A, Matsumoto T, et al. Study of high magnetic anisotropy Co/Pd multilayers for patterned media. J Appl Phys. 2008;103.7:07C502–2.
13. Kubota T, Miura Y, Watanabe D, Mizukami S, Wu F, Naganuma H, et al. Magnetoresistance effect in tunnel junctions with perpendicularly magnetized $D0_{22}$-$Mn_{3-\delta}Ga$ electrode and MgO barrier. Appl Phys Express. 2011;4(4):043002.
14. Kubota T, Mizukami S, Watanabe D, Wu F, Zhang X, Naganuma H, et al. Effect of metallic Mg insertion on the magnetoresistance effect in MgO-based tunnel junctions using D022-Mn3-δGa perpendicularly magnetized spin polarizer. J Appl Phys. 2011;110(1):013915.
15. Sundar RS, Deevi SC. Soft magnetic FeCo alloys: alloy development, processing, and properties. Int Mater Rev. 2005;50(3):157–92.
16. Burkert T, Nordström L, Eriksson O, Heinonen O. Giant magnetic anisotropy in tetragonal FeCo alloys. Phys Rev Lett. 2004;93(2):027203.
17. Andersson G, Burkert T, Warnicke P, Björck M, Sanyal B, Chacon C, et al. Perpendicular magnetocrystalline anisotropy in tetragonally distorted Fe-Co alloys. Phys Rev Lett. 2006;96(3):037205.
18. Yildiz F, Przybylski M, Ma XD, Kirschner J. Strong perpendicular anisotropy in Fe 1−x Co x alloy films epitaxially grown on mismatching Pd (001), Ir (001), and Rh (001) substrates. Phys Rev B. 2009;80(6):064415.
19. Ikeda S, Miura K, Yamamoto H, Mizunuma K, Gan HD, Endo M, et al. A perpendicular-anisotropy CoFeB/MgO magnetic tunnel junction. Nat Mater. 2010;9(9):721–4.
20. Endo M, Kanai S, Ikeda S, Matsukura F, Ohno H. Electric-field effects on thickness dependent magnetic anisotropy of sputtered MgO/$Co_{40}Fe_{40}B_{20}$/Ta structures. Appl Phys Lett. 2010;96(21):2503.
21. Worledge DC, Hu G, Abraham DW, Sun JZ, Trouilloud PL, Nowak J, et al. Spin torque switching of perpendicular Ta/CoFeB/ MgO-based magnetic tunnel junctions. Appl Phys Lett. 2011;98(2):022501.
22. Yamanouchi M, Koizumi R, Ikeda S, Sato H, Mizunuma K, Miura K, et al. Dependence of magnetic anisotropy on MgO thickness and buffer layer in $Co_{20}Fe_{60}B_{20}$/MgO structure. J Appl Phys. 2011;109.7:07C712.
23. Cheng CW, Feng W, Chern G, Lee CM, Wu TH. Effect of cap layer thickness on the perpendicular magnetic anisotropy in top MgO/CoFeB/Ta structures. J Appl Phys. 2011;110(3):033916.
24. Wang Y, Perdew JP. Correlation hole of the spin-polarized electron gas, with exact small-wave-vector and high-density scaling. Phys Rev B. 1991;44(24):13298.
25. Kresse G, Joubert D. From ultrasoft pseudopotentials to the projector augmented-wave method. Phys Rev B. 1999;59(3):1758.
26. Drautz R, Díaz-Ortiz A, Fähnle M, Dosch H. Ordering and magnetism in Fe-Co: dense sequence of ground-state structures. Phys Rev Lett. 2004;93(6):067202.
27. Yang HX, Chshiev M, Dieny B, Lee JH, Manchon A, Shin KH. First-principles investigation of the very large perpendicular magnetic anisotropy at Fe/MgO and Co/MgO interfaces. Phys Rev B. 2011;84(5):054401.
28. Wu D, Zhang Q, Liu JP, Yuan D, Wu R. First-principles prediction of enhanced magnetic anisotropy in FeCo alloys. Appl Phys Lett. 2008;92(5):052503.
29. Miura Y, Ozaki S, Kuwahara Y, Tsujikawa M, Abe K, Shirai M. The origin of perpendicular magneto-crystalline anisotropy in $L1_0$–FeNi under tetragonal distortion. J Phys Condens Matter. 2013;25:106005.
30. He KH, Chen JS, Feng YP. First principles study of the electric field effect on magnetization and magnetic anisotropy of FeCo/MgO (001) thin film. Appl Phys Lett. 2011;99(7):072503.